Nonlinear Finite Element Analysis of Reinforced Concrete Beams with Large Opening under Flexure

Dr. Ihsan A. S. Al-Shaarbaf[1], Nabil A-M. J. Al-Bayati[2], Dhar I. A. Al-Kaisy[3]

Received on :6/6/2005
Accepted on :1/12/2005

Abstract

This paper describes a three- dimensional nonlinear finite element model suitable for the analysis of reinforced concrete Beams with Large Opening under Flexure. The 20-node isoparametric brick elements have been used to model the concrete. The nonlinear equations of equilibrium have been solved using an incremental-iterative technique operating under load control. The solution algorithm used was the modified Newton-Raphson method. The numerical integration has been conducted using the 27-point Gaussian type rule. The reinforcing bars are idealized as axial members embedded within the concrete element and perfect bond between the concrete and the reinforcement has been assumed to occur. The behavior of concrete in compression is modeled using an elasto-plastic work hardening model followed by a perfectly plastic response, which is terminated at the onset of crushing. In tension, a smeared crack model with fixed orthogonal cracks has been used with the inclusion of models for the retained post-cracking tensile stress and the reduced shear modulus. Different types of reinforced concrete beams with large rectangular transverse openings have been analyzed and the finite element solutions are compared with the experimental data. Generally, good agreement has been obtained between the numerical and experimental load-deflection curves and ultimate load. Numerical studies including some material parameters such as concrete compressive strength, amount of longitudinal tensile reinforcement and opening size on the load-deflection response have been carried out to study their effect on the over all behavior of reinforced concrete beams with Large opening under Flexure.The finite element solution revealed that the ultimate load and post-cracking stiffness increase with the increases of concrete compressive strength, increases with the increase of the bottom steel reinforcement amount and decreases with the increase of length or depth of opening.

Keywords: Finite element method; Brick element; Opening beams; Flexural loading.

[1] Assistant Prof., Dept. of Civil Eng. ,College of Eng., Al-Nahrain University, Baghdad.
[2] Assistant Prof., Dept. of Building & Construction Eng., University of Technology.
[3] M. Sc. Civil Engineer, Baghdad – IRAQ.

https://doi.org/10.30684/etj.25.2.8
2412-0758/University of Technology-Iraq, Baghdad, Iraq

التحليل غير الخطي باستخدام طريقة العناصر المحددة للعتبات الخرسانية المسلحة الحاوية على فتحة كبيرة تحت تأثير أحمال الانحناء

الخلاصة

يصف هذا البحث دراسة أنموذجا للتحليل غير الخطي ثلاثي الأبعاد باستخدام طريقة العناصر المحددة للعتبات الخرسانية المسلحة الحاوية على فتحة كبيرة تحت تأثير أحمال الانحناء. وتم حل معادلات التوازن غير الخطية باستخدام طريقة تزايدية – تكرارية تحت سيطرة الحمل، فضلا عن تبني طريقة نيوتن- رافسون المعدلة لإنجاز الحلول الرياضية. وقد أجريت التكاملات العددية باستخدام قواعد التكامل ذات ٢٧ نقطة تكامل حيث تم استخدام العنصر الطابوقي ذو العشرين عقدة لتمثيل الخرسانة، أما حديد التسليح فقد مُثل بعناصر محورية مطمورة داخل العنصر الطابوقي مع افتراض وجود ترابط تام بين الخرسانة وحديد التسليح. وتم تمثيل تصرف الخرسانة تحت تأثير إجهادات الضغط باستخدام النموذج المرن - اللدن ذي التقوية الانفعالية والمتبوع بتصرف لدن تام يستمر لغاية تهشّم الخرسانة. بيد أن تمثيل سلوك الخرسانة تحت تأثير إجهادات الشد أعتمد نموذج التشقق المنتشر وأستعمِل نموذج تصلب الشد لحساب إجهادات الشد المتبقية بعد حدوث التشقق كما استخدم نموذج احتباس القص الذي يقوم بتخفيض قيمة معامل القص المتبقي مع استمرار التحميل في مرحلة ما بعد التشقق. وبعد تحليل أنواع مختلفة من العتبات الخرسانية المسلحة الحاوية فتحات جانبية كبيرة مستطيلة الشكل، قورنت نتائجها المستحصلة مع النتائج المختبرية بدراسة العديد من المتغيرات الخاصة بطريقة العناصر المحددة لمعرفة تأثيرها. كما درس تأثير مقاومة ضغط الخرسانة، وكمية حديد التسليح الطولي، وحجم الفتحة، ومن خلال دراسة العلاقة بين الحمل والهطول، ومقدار الحمل الأقصى كانت نتائج التطابق جيدة بين الطريقة التحليلية والفحص العملي. أظهرت طريقة العناصر المحددة في التحليل أن الحمل الأقصى يزداد مع زيادة مقومة انضغط الخرسانة ويزداد مع كمية حديد التسليح الطولي السفلي ويقل مع زيادة طول وعمق الفتحة.

1-Introduction

In modern building construction, utility ducts and pipes are accommodated in the space above the false ceiling. Passing these ducts through openings in the floor beams eliminates a significant amount of dead space and results in a more compact and economical design. However, the effects of openings on the strength and behavior of the beams must be considered. Including transverse openings in the web of a reinforced concrete beam induces high stress concentration at opening corners, reduces beam stiffness, and alters the simple beam behavior to a more complex one. Therefore, while providing a large opening, the effects on ultimate and service load behaviors of the beam must be properly accounted for in design.

In the past, a lot of research had been carried out to study the behavior of reinforced concrete beams with transverse openings. The investigations[1-4] dealt with the behavior of reinforced concrete beams with transverse rectangular and circular opening under flexure, shear, torsion and the combined effect of (flexure and torsion) or (flexure and shear). Two types of transverse openings were tested, the small opening and the large opening, a circular opening may be considered as large when its diameter exceeds a quarter of the depth of the web because the presence of such openings reduces the strength of the beam [4]. These investigations also dealt with

the opening length, depth, eccentricity, and location along the beam length.

2-Research Significance

The main objective of this study is to investigate the behavior of reinforced concrete beams with large opening under flexure using a three-dimensional nonlinear finite element model. The 20-node isoparametric brick elements are used to model the concrete, while the steel bars are modeled as axial members embedded within the concrete brick element, assuming perfect bond between the concrete and steel. The material nonlinearity due to cracking of concrete, crashing of concrete, yielding of reinforcement and nonlinear stress-strain response of reinforced concrete beams with large opening in compression are considered.

The behavior of reinforced concrete beams with large opening in compression is simulated by an elasto-plastic strain-hardening model followed by perfectly plastic plateau, which is terminated at the initiation of crushing. In tension, a smeared crack model with fixed orthogonal cracks has been used to simulate the behavior of concrete.

3-Finite Element Program

The formulation and a comprehensive discussion of the finite element method have been described extensively in several standard texts[5,6,7,8] In this study, concrete model is presented by using the 20-node quadratic brick elements shown in Fig.(1), while the reinforcing bars are simulated as one dimensional elements subjected to axial force only. These elements are embedded within the concrete brick elements and perfect bond is assumed to occur between the two materials. Full details on both thory and performance of the brick element are given in reference[9].

An elasto-plastic strain-hardening model followed by perfectly plastic response simulates the behavior of concrete in compression. This response is terminated at the onset of crashing. In tension, a fixed smeared crack model has been used with a tension-stiffening model to represent the retained post-cracking tensile stresses and a shear-retention model that modifies the shear modulus of rigidity of concrete due to cracking.

In this study, a plasticity-based model is adopted for the nonlinear three-dimensional finite element analysis of reinforced concrete beams with large opening under static loads. The plasticity model in compression state of stress has the following[9]:

1. Yield Criterion:

The yield criterion incorporated in the present model can be expressed as:

$$f(\{s\}) = f(I_1, J_2) = CI_1 + \sqrt{(CI_1)^2 + 3bJ_2} = s_o \quad ...(1)$$

where C and β are material parameters and I_1, and J_2 are the first and second deviatoric stress invariants, and σ_o is the equivalent effective stress taken from uniaxial tests.

$$\sigma_o = C_p f'_c \quad ...(2)$$

Where C_p is a plasticity coefficient used to mark the initiation of plasticity deformation ($0.0 < C_p < 1.0$)

2. Hardening Rule :

In this present research work, an isotropic hardening rule is adopted. The rule implies a uniform expansion of the initial yield surface as the plastic deformation increase.

Therefore, from Eq.(1), the subsequent loading functions may be expressed as:

$$f(\{s\}) = cI_1 + \sqrt{(cI_1)^2 + 3bJ_2} = \bar{s} \quad \ldots(3)$$

where $\bar{s}$ represent the stress level at which further plastic deformation will occur and termed as the effective stress or the equivalent uniaxial stress at that level. In the present model, a parabolic stress-strain curve is used for the equivalent uniaxial stress-strain relationship beyond the limit of elasticity (C_p f'$_c$) and can be expressed as:

for $C_p f'_c \le \bar{s} \le f'_c$

$$\bar{s} = C_p f'_c - E e_p + \sqrt{2E^2 e'_o e_p} \quad \ldots(4)$$

where, E is the initial Young's modulus, ε_p is the plastic strain component, ε'_o is the total strain corresponding to the parabolic part of the curve given by:

$$e'_o = 2(1 - C_p)\frac{f'_c}{E} \quad \ldots(5)$$

For normal strength concrete, a value of 0.3 is assumed for the plastic coefficient C_p.

3. Flow Rule :

In this rule the plastic strain increment vector is assumed to be normal to the yield surface. The plastic strain increment vector can be expressed as:

$$d\{e_p\} = dl\,\frac{\partial f(s)}{\partial s} \quad \ldots(6)$$

where dl is a positive scalar hardening parameter, which can vary throughout the straining process. The gradient of the yield-loading surface ($\partial f(s)/\partial s$) defines the direction of the plastic-strain increment vector $d\{e_p\}$ while the length is determined by the loading parameter dl.

The elasto-plastic incremental stress-strain relationship can be expressed as:

$$d\{s\} = [D]_{ep}\ d\{e\} \quad \ldots(7)$$

where,

$$[D]_{ep} = \left[[D] - \frac{[D]\{a\}\{a\}^T[D]}{H' + \{a\}^T[D]\{a\}}\right] \quad \ldots(8)$$

where [D] is the elastic constitutive matrix, H' is the hardening parameter which represents the slope of the effective stress-plastic strain curve and {a} is the flow vector which is the yield function derivatives with respect to the stress components.

4. Crushing Condition :

The crushing criterion is usually obtained by converting the yield criterion in Eq. (1), which is written in terms of stresses, directly into strains, thus:

$$C.I'_1 + \sqrt{(C.I'_1)^2 + 3b.J'_2} = e_{cu} \quad \ldots(9)$$

where I'_1 and J'_2 are the first strain invariants and the second deviatoric strain invariant and e_{cu} is the ultimate crushing strain of concrete, extrapolated from a uniaxial compression test.

In tension, linear elastic behavior prior to cracking is assumed. A smeared crack model with fixed orthogonal cracks is adopted to represent the fractured concrete. The model has been described in terms of the following:

1. Cracking Criterion:

Cracking occurs if the principal tensile stress exceeds the limiting tensile strength of concrete. Because

of the lack of interaction between the orthogonal planes caused by cracking, Poisson's ratio, ν, is set to zero and a reduced shear modulus b_1G is employed to model the shear strength deterioration. Therefore, the incremental stress-strain relationship in the local material axes may be expressed as:

$$\begin{Bmatrix}\Delta s_1\\ \Delta s_2\\ \Delta s_3\\ \Delta t_{12}\\ \Delta t_{23}\\ \Delta t_{13}\end{Bmatrix}=\begin{bmatrix}E_1 & 0 & 0 & 0 & 0 & 0\\ 0 & E/1-n^2 & nE/1-n^2 & 0 & 0 & 0\\ 0 & nE/1-n^2 & E/1-n^2 & 0 & 0 & 0\\ 0 & 0 & 0 & b_1G & 0 & 0\\ 0 & 0 & 0 & 0 & G & 0\\ 0 & 0 & 0 & 0 & 0 & b_1G\end{bmatrix}\begin{Bmatrix}\Delta e_1\\ \Delta e_2\\ \Delta e_3\\ \Delta g_{12}\\ \Delta g_{23}\\ \Delta g_{13}\end{Bmatrix} \quad ...(10)$$

Equation (10) may be written as:

$$\Delta\{s\}=[D_{cr}]\Delta\{e\} \quad \ldots(11)$$

where $[D_{cr}]$ is the material stiffness in local material axes.

2. Post-Cracking Formulation:

Since the cracked concrete can still initially carry some tensile stresses in the direction normal to the crack, the *tension-stiffening* effect has to be considered. The gradual release of concrete tensile stresses normal to the cracked plane is represented by an average stress-strain curve, and expressed as [7]:

a) For $e_{cr} \le e_n \le a_1 e_{cr}$

$$s_n = a_2 s_{cr}[a_1 - e_n/e_{cr}]/[a_1 - 1.0] \quad ...(13)$$

b) For $e_n > a_1 e_{cr}$

$$s_n = 0.0 \quad \ldots(14)$$

where ε_{cr} is the cracking strain associated with the cracking stress, σ_{cr}, and α_1 and α_2 are the tension-stiffening parameters. α_1 represents the rate of stress release as the crack widens; α_2 represents the sudden loss of stress at instant of cracking.

3. Shear-Retention Model:

A *shear retention model* is usually used to take into account the capacity of the cracked concrete to transfer shear across the crack. In the present study, and for three-dimensional analysis, a reduction factor β has been used across the cracked planes, to reduce the shear stiffness at the cracked sampling points. Before cracking, a value of unity is assigned to the shear reduction factor β. As the crack propagates, the shear reduction factor is taken to be linearly decreased with the strain normal to the cracked plane, which represents the crack width. When the cracks have sufficiently opened, a constant value is assigned to β to account for dowel action. The shear retention model can be expressed as:

(a) For $e_{cr} > e_n$

$$b = 1.0 \quad \ldots(15)$$

(b) For $e_{cr} \le e_n \le g_1 e_{cr}$

$$b = \frac{g_2 - g_3}{g_1 - 1}[g_1 - e_n/e_{cr}] + g_3 \quad .(16)$$

(iii) For $e_n > g_1 e_{cr}$

$$b = g_3 \quad \ldots(17)$$

where, γ_1, γ_2, and γ_3 are the shear retention parameters. γ_1, represents the rate of decay of shear stiffness as the crack widens; γ_2 represents the sudden loss in shear stiffness at the instant of cracking, and γ_3 represents the residual shear stiffness due to dowel action.

In the current study, the uniaxial stress-strain behavior of steel reinforcement has been simulated by

an elastic-linear work hardening model for both two and three-dimensional nonlinear finite element analyses.
Details of the finite element models are given in reference [10].

4-Analysis of Reinforced Concrete Beams with Large Opening under Flexure

In this section, an investigation on the nonlinear behavior and the load carrying capacity of reinforced concrete beams with large opening under flexure is conducted using the adopted nonlinear finite element model. The aim of this section is to verify the efficiency and accuracy of the model to simulate the load-deflection response of reinforced concrete beams with large opening at the elastic, cracking and post-cracking stages of behavior and the response at ultimate loads.

The experimental work has been considered in this study was conducted by Mansur et al [3].

4-1-Description of Mansur et al Beams

In this work, the experimental flexural test were conducted on four simply supported beams, the beams were designated as R2, R3, R6 and R11. The beams were rectangular and their dimensions, positions of load application, amount and arrangement of longitudinal reinforcement were held constant. The opening size, its location, and arrangement of transverse reinforcement were varied. The length of the openings ranged from 600mm in beam R2 to 800mm in beams R3, R6, and R11. In addition, the depth of the openings ranged from 140mm in beam R6 to 180mm in beams R2, R3, and R11. The selected beams R2, R3, R6, and R11, differed in their length, depth, and location of opening along the beam length. Table (1) illustrates the properties of the selected beams. Fig. (2) and Table (2), show details of reinforcement. Deformed steel bars of 16, 13, and 10mm diameter and plain bars of 6mm diameter were used. The yield stresses of these bars were 499, 420, 446, and 355MPa, respectively. The longitudinal bars were continued to the end of the beams. Closed stirrups of 6mm diameter bars were employed. In the solid part of the beam, stirrup spacing was kept constant at 100mm for all the beams. However, in the regions below and above the opening, the spacing of the stirrups was varied for different specimens. In addition, the corner shear reinforcement consisted of full-depth closed stirrups, which were placed as close to the side of the opening as possible, Table (1). During the experimental tests the deflections of the beams were recorded for different stages of loading at the right end of the opening. At each increment, the load was kept constant for a while to allow the beam to stabilize. Then the dial gage reading was recorded. Close to failure stage, the dial gage was removed and the load values were recorded up to the ultimate value.

4-2-Finite Element Idealization and Material Properties

By taking advantage of symmetry, a segment representing half of the beam has been considered in the finite element analysis, as shown in Fig. (3). The selected segment was modeled using 52-twenty node isoperimetric brick elements. The 27-point integration

rule has been generally used to carry out the numerical integration.

The external loads were initially applied in equal increments. The loading increments at stages close to the ultimate load were smaller than those used at early stages of loading. The finite element mesh, boundary and symmetry conditions used in the analysis are shown in Fig.(4). Material properties and numerical parameters of the tested beams are listed in Table (3).

4-3-Results of Analysis

In this section, the numerical results obtained for the four beams are compared with the experimental data as shown in Figs. (5) to (8). The ratio of the experimental ultimate loads to the corresponding values of the numerical ultimate load for beams R2, R3, R6 and R11 were 1.075, 1.005, 1.122, and 1.006 respectively. Generally good agreement was obtained in the pre-cracking and post-cracking stages of behavior for all tested beams. The experimental and numerical ultimate loads and the ratio of the experimental ultimate load to the numerical ultimate load for the tested beams are listed in Table (4).

4-4-Parametric Study

In this section, a parametric study includes the grade of concrete, amount of longitudinal reinforcement, and opening sizes. The numerical study, which has been conducted in this section, is presented on two of the analyzed beams R2 and R3.

4-4-1-Influeance of Grade of Concrete

Figs. (9) and (10) show the effect of using higher values of compressive strength of concrete, on the load-deflection behavior of beams R2, and R3. Different values of compressive strength of concrete were used in these analyses. The figures indicate that the increase in the magnitude of compressive strength of concrete, from the value given in the experimental work (30.4 MPa, for beam R2 and 33.5 MPa for beam R3) to 50.0 and 80.0 MPa leads to appreciable increase of the predicted post-cracking stiffness of the beams. The increase in the value of the compressive strength of concrete results in a substantial increase in the ultimate load. The collapse loads obtained from this study are listed in Table (5).

4-4-2-Effect of Amount of longitudinal Reinforcement

The cross-section of beams R2 and R3 with three different amounts of bottom steel bars are shown in Fig. (11). In (case-1), (case-2) and (case-3) the areas of longitudinal bottom steel were 530.93, 667.59 and 804.25 mm^2 respectively. Case-2 represents the beam cross-section with the same amount of steel bars as used in the experimental tests of beams R2 and R3. Figs. (12) and (13) exhibit the effect of variation of the amount of bottom steel bars on the load-deflection response of reinforced concrete beams with large opening. The increase in the amount of longitudinal bottom steel substantially affects the overall shape of the load-deflection curves and the load carrying capacity. Table (6) shows the influence of the longitudinal bottom steel reinforcement on the ultimate load capacity.

4-4-3- Effect of Opening Length

The effect of varying the length of opening on the load-deflection

response and ultimate load capacity of beam R3 was numerically carried out. In this study the depth of the opening was kept constant while its length increased from 400mm to 1200mm by increments of 200mm each.

Fig. (14) reveals that the decrease in the opening length results in a substantial increase in the ultimate load. The collapse loads obtained from this study are listed in Table (7) together with the experimental value.

4-4-4- Effect of Opening Depth

The effect of opening depth on the load-deflection response and ultimate load capacity, numerical tests were mainly carried out by analyzing beam R_3, where the length of the openings was kept constant but its depth was increased from 100mm to 260mm by increments of 40mm each. Fig (15) shows that, as the depth of opening increases, the load carrying capacity is substantially decreased. The predicted values of the ultimate loads obtained from the finite element analysis for different values of the opening depth are compared with the experimental value in Table (8).

4-4-5 Effect of Opening Location

To study the effect of opening location along the span on the load-deflection response and ultimate load capacity, numerical tests were mainly carried out by analyzing beam R_3, where the position of the applied load was kept constant but the distance between the center of opening and the left support was taken as 1000, 1500 and 2000mm.

Fig (16) shows the relationship between the load and the deflection under the load. The predicted values of the ultimate load capacity obtained from the finite element analysis for distances of 1000, 1500 and 2000mm from left support were 143.3, 113.3 and 123kN respectively. Also, as the distance between the applied load and the nearest end of the opening decreases the load capacity is also decreased.

Figs. (17), (18) and (19) show the deflected shape along beam length at the ultimate load level. It is worth noting that the maximum deflection occurred at the opening edge.

4-5 Distribution of Concrete Stresses at Beam Cross-Sections

Distribution of concrete bending stresses along the depth of different cross-sections of beams R_2 and R_3 has been numerically investigated at two stages of loading. The selected of stages of loading were 100kN (before yielding) and the ultimate loads of beams R_2 and R_3 (169.8kN and 143.3kN respectively). In this study the bending stress distributions at four sections were investigated Figs.(20,22). These sections were close to the center of the opening, before and after the right end of the opening, and the point of load application. Figs.(21-a) to (21-d) show the distribution of bending stresses for beam R_2 and Figs.(23-a) to (23-b) for beam R_3 respectively. For both beams the maximum values of compressive bending stress occurred at the top face of the cross-section close to the point of load application and the sections located at right end of the opening. Figs.(21-a, b and c) and Figs.(23-a, b and c) reveal that, the compressive stress occurred at the top face of the bottom chord of the opening.

5-Conclusions

1. The three-dimensional nonlinear finite element model used in the present research work is able to simulate the behavior of reinforced concrete beams with large transverse openings subjected to flexure. The numerical analyses carried out showed that the predicted load-deflection curves are in good agreement with the experimental results for different beams with different sizes of openings.
2. The finite element solutions show that the value of concrete compressive strength can significantly influence the post-cracking stiffness and the ultimate load. The results revealed that an increase of 6.8% and 14.8% in the ultimate load has been achieved for beams R_2 and R_3 respectively, when the compressive strength of concrete is increased from 50MPa to 80MPa.
3. The analysis result of using different bottom steel bars in reinforced concrete beams with transverse large opening under flexure show that the increase in the amount of bottom steel reinforcement from 530.9 mm^2 to 667.6 mm^2, leads to an increase of 35% and 19% in the ultimate load of beams R2 and R3 respectively. On the other hand the increase in the amount of the steel of steel reinforcement from 530.9 mm^2 to 804.3 mm^2 leads to an increase of 58% and 35% in the ultimate load of beams R_2 and R_3 respectively.
4. For beam R_3, it was found that the variation of the opening size has a significant effect on the load-deflection behavior and ultimate load capacity. The ultimate load capacity increases by about 22% when the opening length decreases from 800mm to 400mm. While, it decreases by 32% when the opening length increases from 800mm to 1200mm. Also, the ultimate load capacity increases by about 14% when the opening depth decreases from 180mm to 100mm, and it decreases by 46% when the opening depth increases from 180mm to 260mm.
5. For the case study carried out in this work it is found that the deflected shape along the beam length indicates that the maximum deflection of reinforced concrete beams with large opening occurs at the opening edge.
6. The finite element solutions reveal that as the distance between the applied load and the nearest end of the opening decreases the load carrying capacity is also decreased.
7. For beams R_2 and R_3 the stress distribution along the longitudinal bottom bars of beams with large rectangular transverse opening showed that the maximum values of tensile stress of longitudinal reinforcement occurred at the point of load application and at the edges of the opening. It is found that the reinforcing bars reach their yielding stresses at these locations.

References

1. Mansur M.A., and Hasnat A. "Concrete Beams with Small Openings under Torsion" Journal of the Structural Division, ASCE, Vol. 105, No. ST11, November 1979, pp. 2433-2447.

2. Mansur M.A., and Paramasivam P., "Reinforced Concrete Beams with Small Opening in Bending and Torsion" ACI Structural Journal, Vol. 81, No. 2, March-April 1984, pp.180-185.
3. Mansur M.A., Tan K.H., and Lee S.L., "Design Method for Reinforced Concrete Beams with Large Openings" ACI Structural Journal, Vol. 82, No. 4, July-August 1985, pp. 517-524.
4. Mansur M.A., "Effect of Openings on the Behavior and Strength of R/C Beams in Shear" Cement and Concrete Composites, 20 (1998), pp. 477-486.
5. Oden, J. T., "Finite Elements of Nonlinear Continua", McGraw-Hill Book Company, New York, 1972.
6. Zienkiewicz, O. C., "The Finite Element Method", 3rd Edition, McGraw-Hill Book Company, New York, 1977.
7. Cook, R. D., "Concepts and Applications of Finite Element Analysis", 2nd Ed., John Wiley and Sons, New York, 1981.
8. Bathe, K. J., "Finite Element Procedures", Prentice-Hall, Inc., 1996.
9. Al-Shaarbaf I.A.S., "Three Dimensional Nonlinear Finite Element Analysis of Reinforced Concrete Beam in Torsion" Ph. D. Thesis, University of Bradford, 1990, 323 pp.
10. Al-Kaisy D.I.A. "Nonlinear Finite Element Analysis of Reinforced Concrete Beams with Large Opening under Flexure" M.Sc. Thesis, University of Technology, 2005.

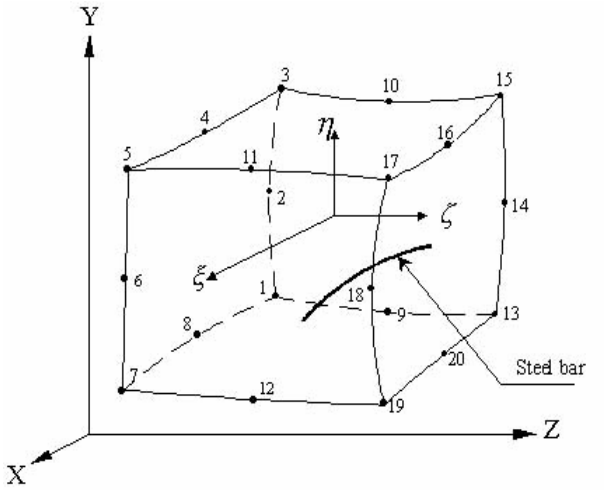

Fig.(1) 20-node brick element

Table (1) Dimensions and stirrup properties used for Mansur et al, beams

Specimen	l, mm	D_t, mm	d_o, *mm*	D_b, mm	a, mm	*Stirrup* spacing (s), mm	Corner closed stirrups reinforcement, mm
R_2	*600*	*110*	*180*	*110*	*700*	*40*	*1-10*
R_3	*800*	*110*	*180*	*110*	*600*	*40*	*1-10*
R_6	*800*	*130*	*140*	*130*	*600*	*50*	*1-10*
R_{11}	*800*	*110*	*180*	*110*	*600*	*40*	*1-10*

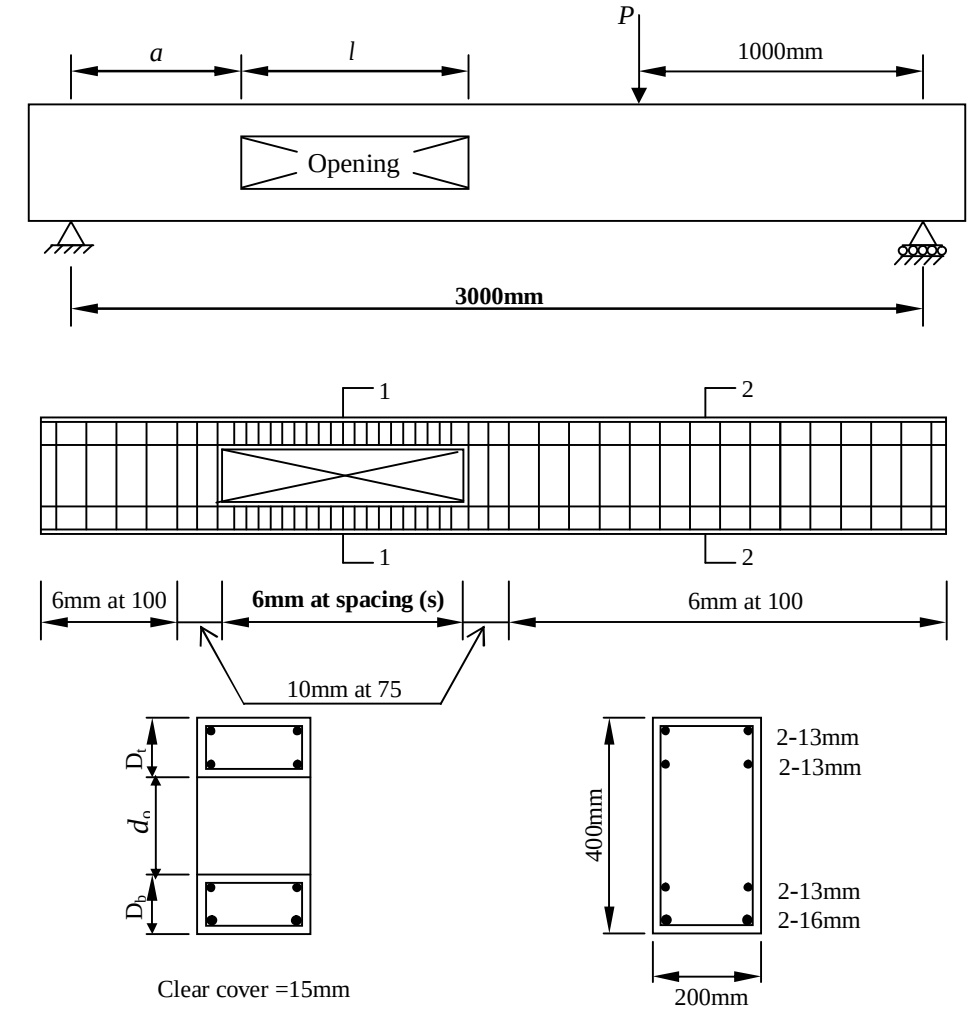

Fig. (2) Dimensions and reinforcement details of Mansur et al, beams

Table (2) Steel bars properties used for Mansur et al, beams

Diameter of bars, mm	Yield stress, f_y (MPa)	Young's Modulus, E_s (GPa)
6	355	200
10	446	200
13	420	200
16	499	200

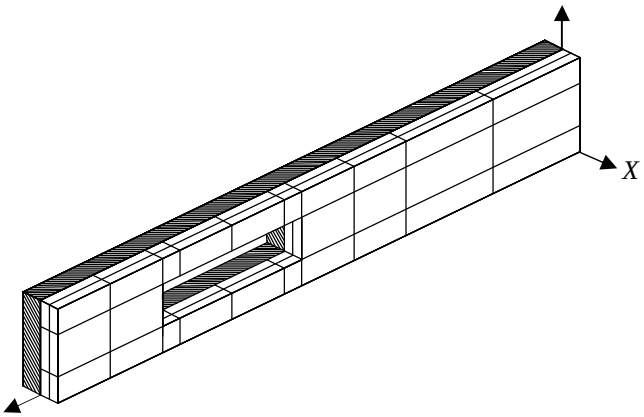

Fig. (3) Finite element mesh and symmetry conditions used for Mansur et al,

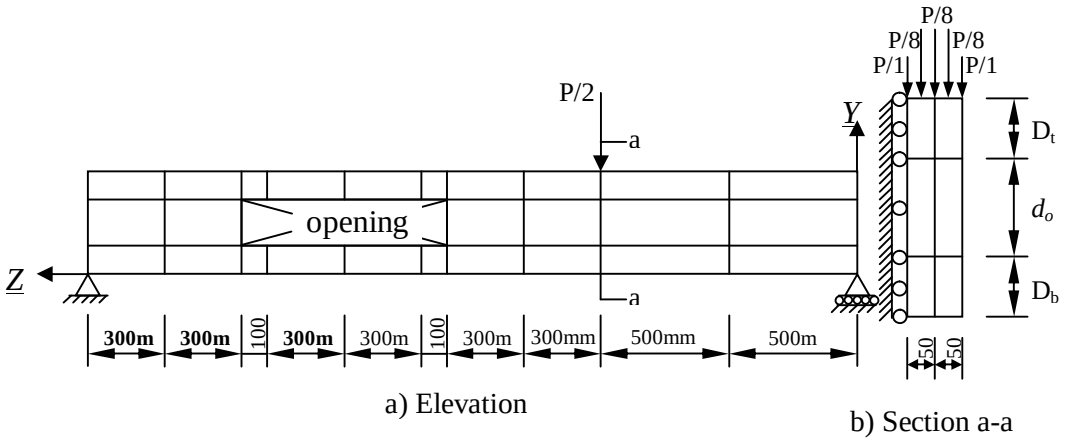

Fig. (4) Finite element mesh and boundary conditions used for Mansur et al, beams

Table (3) Concrete properties and additional material parameters used for Mansur et al, beams

Beam Designation	R2	R3	R6	*R11*
Young's Modulus, E_c (GPa)	25.91	27.20	25.66	25.22
$f_c^{/}$ (MPa) ,Compressive Strength	30.4	33.5	29.8	28.8
Tensile Strength, F_t (MPa)	2.37	2.48	2.34	2.30
Poisson's Ratio, v	0.2	0.2	0.2	0.2
Uniaxial Crushing Strain	0.005	0.005	0.005	0.005

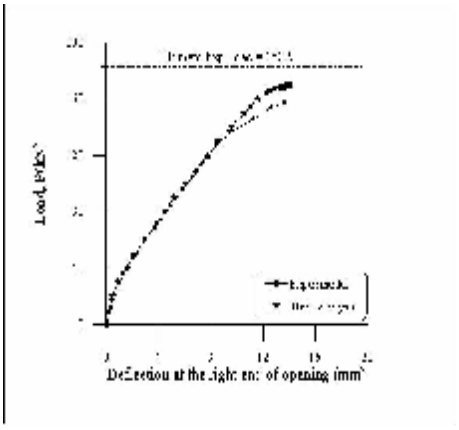

Fig. (5) Experimental and numerical response or for beam R2

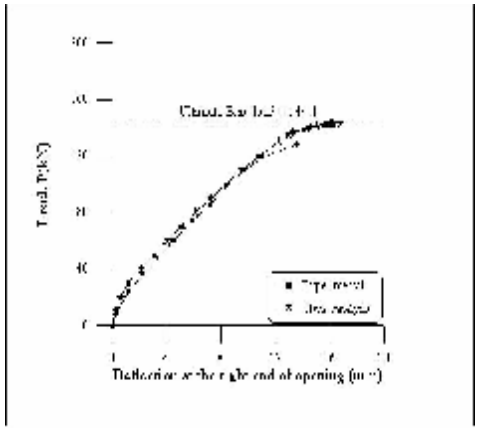

Fig. (6) Experimental and numerical response for beam R3

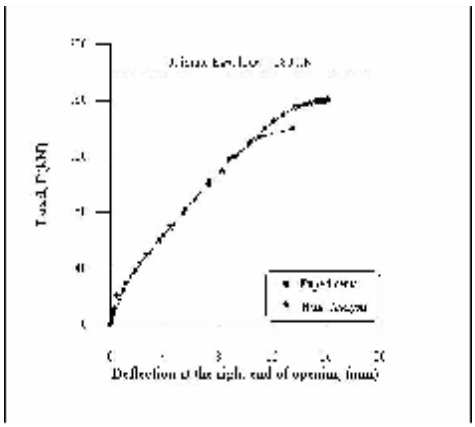

Fig. (7) Experimental and numerical response for beam R6

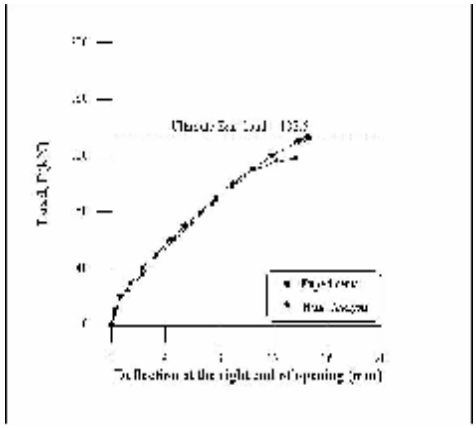

Fig. (8) Experimental and numerical response for beam R11

Table (4) Comparison between numerical and experimental ultimate loads of Mansur et al, beams

Beam	Analytical ultimate Load, P_{UA} (kN)	Experimental ultimate Load, P_{UE} (kN)	P_{UE}/P_{UA}
R_2	169.8	182.5	1.075
R_3	143.3	144.1	1.005
R_6	160.4	180.0	1.122
R_{11}	132.7	133.5	1.006

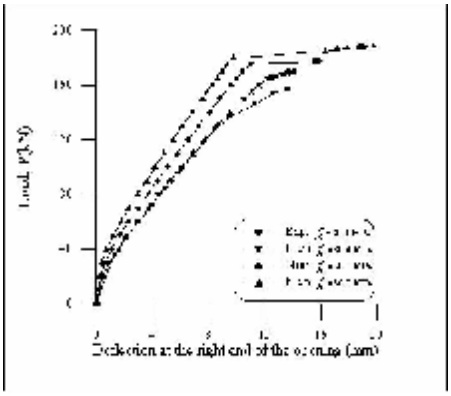

Fig. (9) Effect of the concrete compressive strength on the load-deflection behavior of beam R2

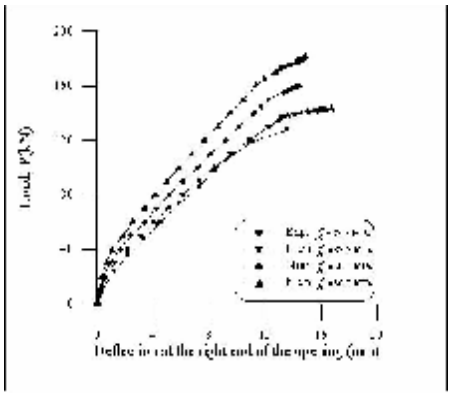

Fig. (10) Effect of the concrete compressive strength on the load-deflection behavior of beam R3

Table (5) Effect of the grade of concrete on the analytical ultimate load capacity of beams R_2 and R_3

Beam (R_2) , f'_c (MPa)	Exp. ultimate load, P_{UE} (kN)	Num. ultimate load, P_{UN} (kN)	$\frac{P_{UN}}{(169.8)}$	Beam (R_3) , f'_c (MPa)	Exp. ultimate load, P_{UE} (kN)	Num. ultimate load, P_{UN} (kN)	$\frac{P_{UN}}{(143.3)}$
30.4	182.5	169.8	1.000	33.5	144.1	143.3	1.000
50.0	_	177.6	1.046	50.0	_	159.9	1.116
80.0	_	189.2	1.114	80.0	_	181.2	1.264

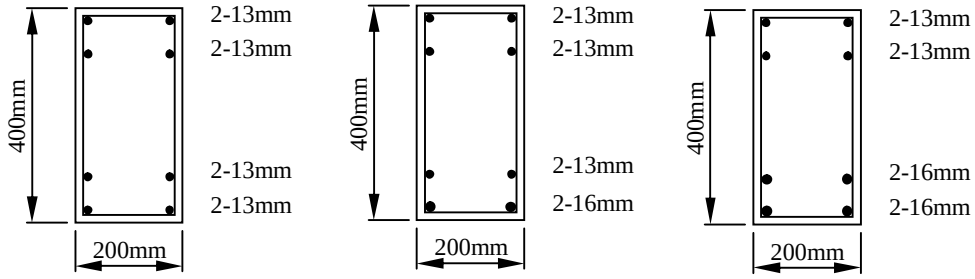

Fig. (11) Amount of longitudinal bottom steel reinforcement used in numerical analysis of beams R_2 and R_3

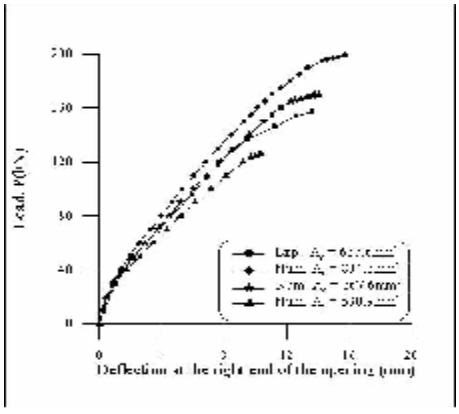

Fig. (12) Effect of the longitudinal tensile reinforcement on the load-deflection behavior of beam R2

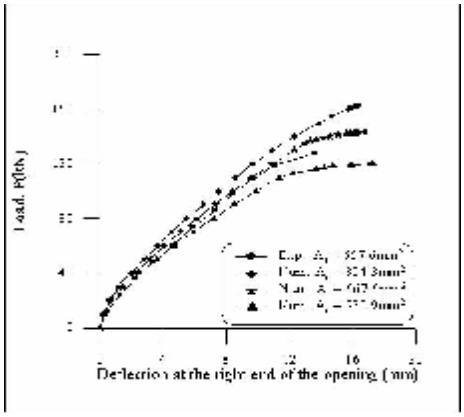

Fig. (13) Effect of the longitudinal tensile reinforcement on the load-deflection behavior of beam R3

Table (6) Effect of the longitudinal bottom steel reinforcement on the analytical ultimate load capacity of beams R2 and R3

			Beam R2		Beam R3	
Case	Arrangement of steel bottom bars	Area of bottom steel bars (mm^2)	Num. ultimate load, P_{UN} (kN)	$P_{UN}/(126.2)$	Num. ultimate load, P_{UN} (kN)	$P_{UN}/(120.2)$
1	**2-13** **2-13**	**530.9**	**126.2**	**1.00**	120.2	1.00
2	2-13 2-16	667.6	169.8	1.35	**143.3**	**1.19**
3	2-16 2-16	804.3	199.2	1.58	**162.6**	**1.35**

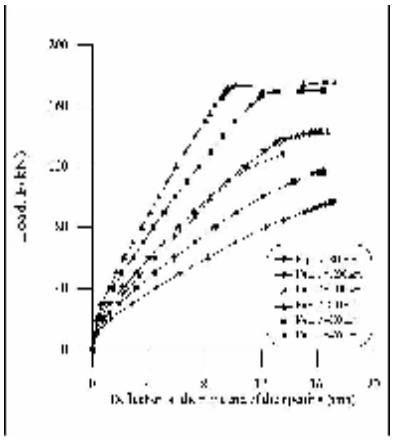

Fig. (14) Effect of opening length on the load-deflection behavior of beam R3

	Opening Length, (mm)	Opening Depth, (mm)	Num. ultimate Load, P_{UN} (kN)	$P_{UN}/(143.3)$
Beam R3	400	180	175.2	1.22
	600	180	170.9	1.19
	800	180	143.3	1.00
	1000	180	116.7	0.81
	1200	180	97.2	0.68

Table (7) Effect of opening length on the analytical ultimate load capacity of beam R3

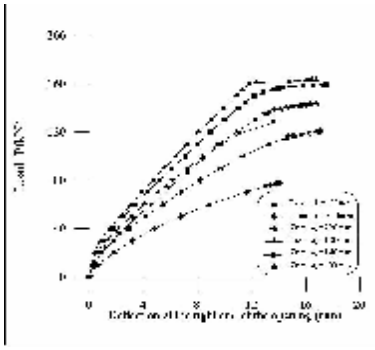

Fig. (15) Effect of opening depth on the load-deflection behavior of

	Opening Length, (mm)	Opening Depth, (mm)	Num. ultimate Load, P_{UN} (kN)	$P_{UN}/(143.3)$
Beam R3	800	100	163.3	1.14
	800	140	159.2	1.11
	800	180	143.3	1.00
	800	220	120.7	0.84
	800	260	77.9	0.54

Table (8) Effect of opening depth on the analytical ultimate load capacity of beam R3

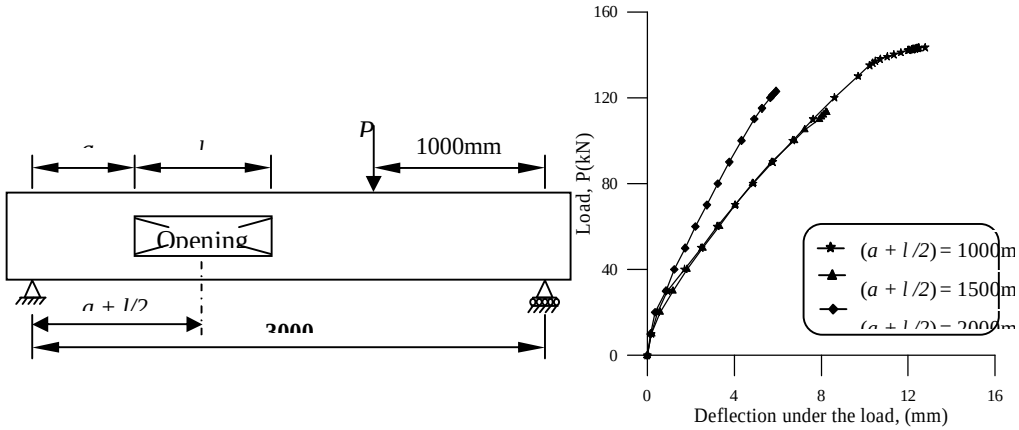

Fig. (16) Effect of opening location on the load-deflection behavior of beam R_3

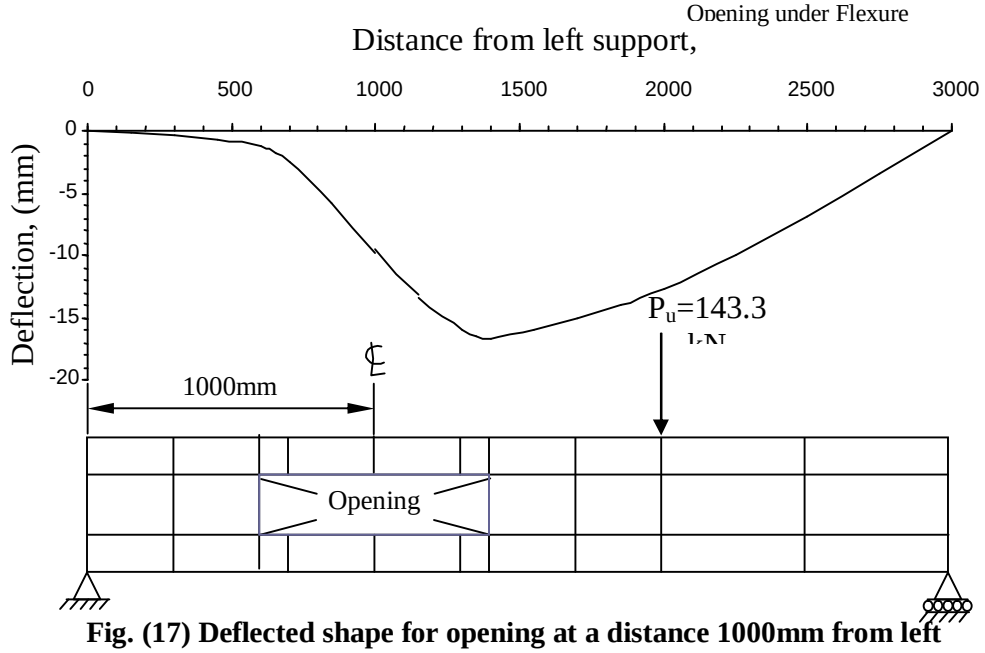

Fig. (17) Deflected shape for opening at a distance 1000mm from left support

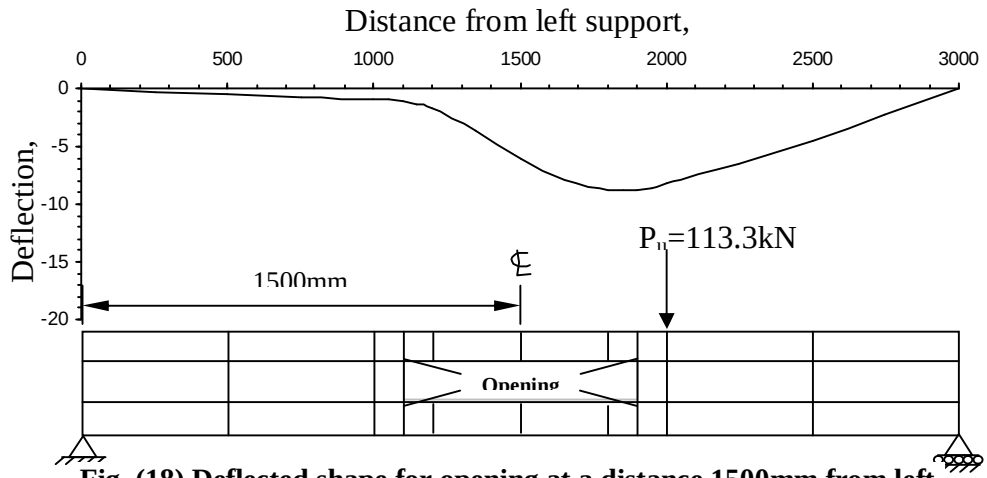

Fig. (18) Deflected shape for opening at a distance 1500mm from left support

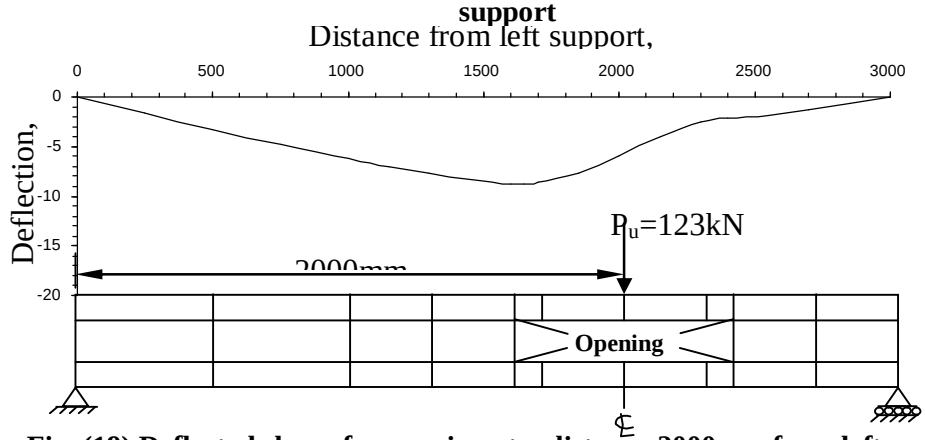

Fig. (19) Deflected shape for opening at a distance 2000mm from left support

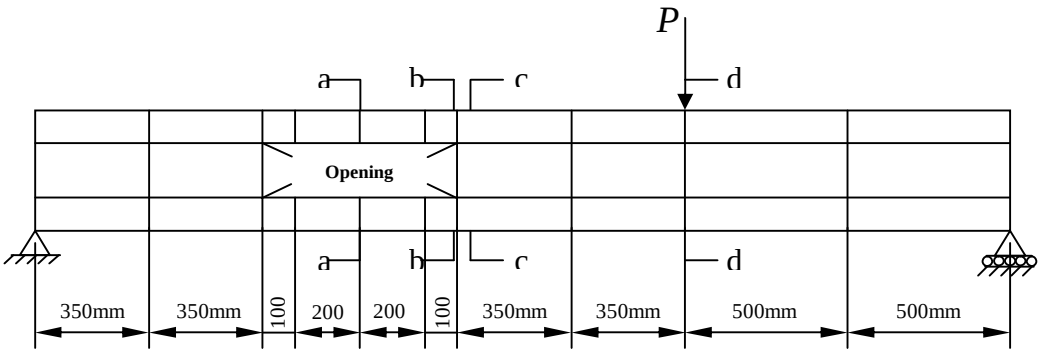

Fig. (20) Positions of studied sections for beam R_2

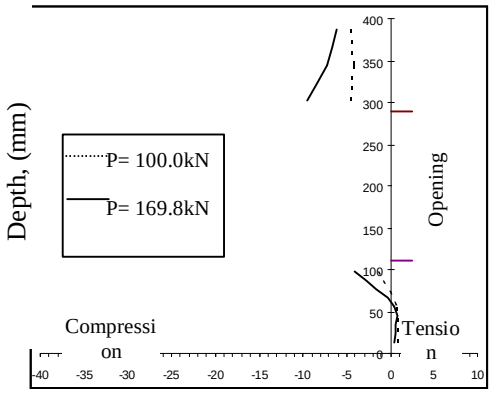

Fig. (21-a) Section (a-a)

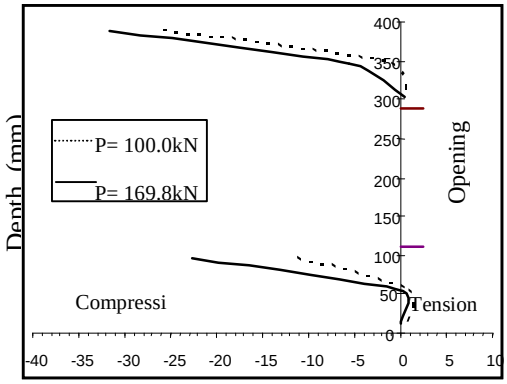

Fig. (21-b) Section (b-b)

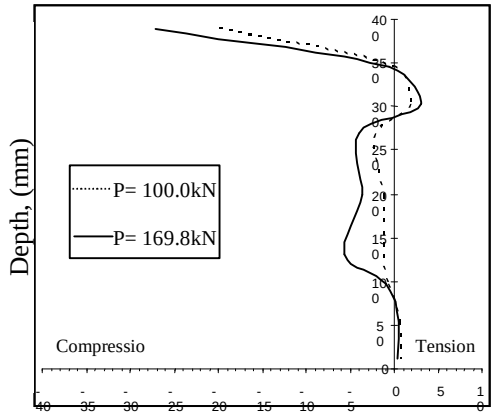

Fig. (21-c) Section (c-c)

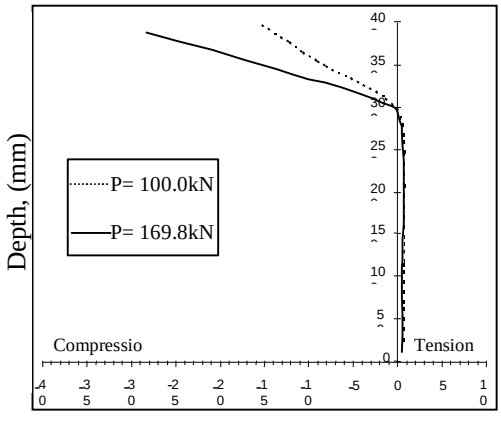

Fig. (21-d) Section (d-d)

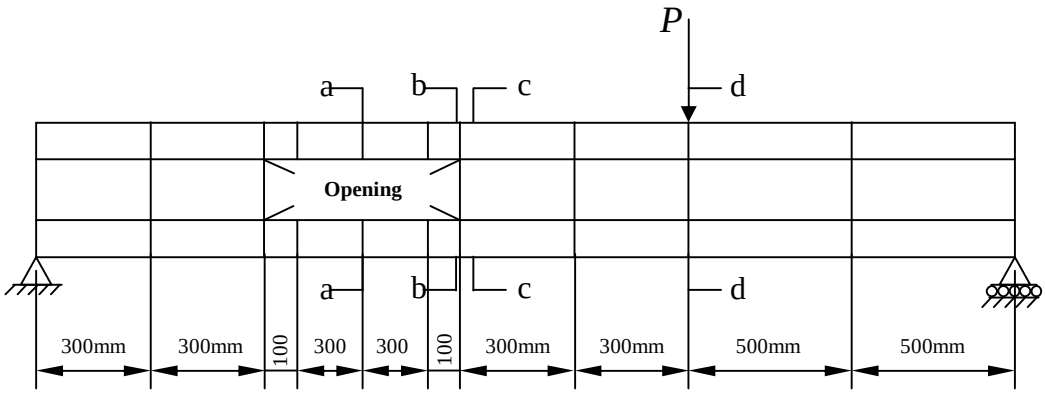

Fig. (22) Positions of studied sections for beam R_3

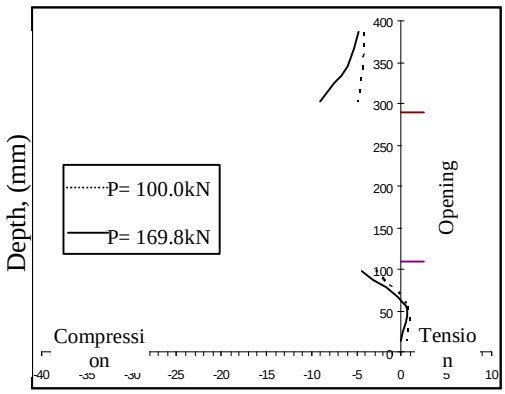

Fig.(23-a) Section (a-a)

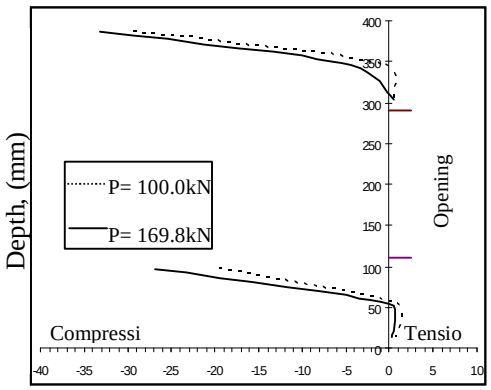

Fig.(23-b) Section (b-b)

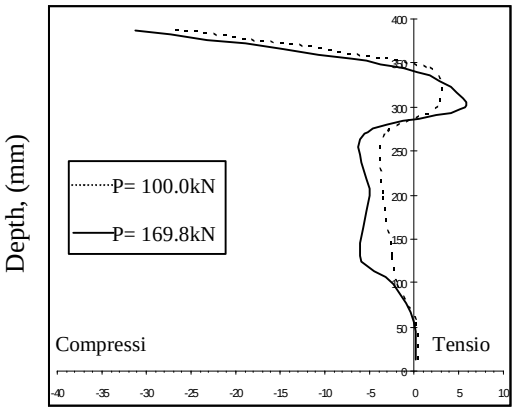

Fig.(23-c) Section (c-c)

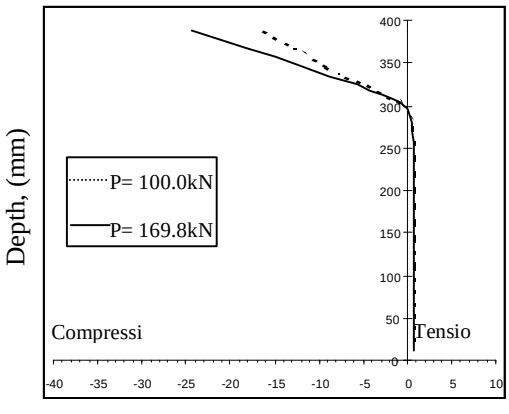

Fig.(23-d) Section (d-d)